JPEDAV (2006) 27:102-112
DOI: 10.1361/105497106X92871
1547-7037/$19.00 ©ASM International

Design Criteria for High-Temperature Steels Strengthened with Vanadium Nitride

V.A. Yardley and Y. de Carlan

(Submitted December 13, 2004; in revised form November 11, 2005)

Fe-8-12Cr ferritomartensitic steels are widely used in the power generation, petrochemical, and nuclear industries where they are subject to high operating temperatures and stresses. Resistance to creep deformation is therefore a critical materials property. One method of providing creep resistance is to precipitate a fine, homogeneous distribution of vanadium nitride (VN) particles in the matrix. Maximizing this precipitation hardening effect requires a high nitrogen content, but this could cause gas bubble formation during conventional fabrication processes. It is therefore necessary to determine how much N can be added without encountering such problems. Phase stability calculations, using Thermo-Calc, were carried out to find high-N compositions, to optimize the fraction of VN and the fabrication route for obtaining fine particles. Several experimental compositions, including nine high-nitrogen alloys, were fabricated as ingots; out of these, two exhibited porosity. Thermo-Calc predicts that, in all of the high-nitrogen alloys, nitrogen gas is a stable phase around the solidus temperature. It is evident that porosity cannot simply be predicted from the presence of the gas phase on the equilibrium diagram. However, detailed analysis of the equilibrium phases predicted in these alloys, including their variation with composition, allowed a porosity criterion to be obtained. This criterion links porosity formation to the nature of the liquid-to-solid transformation. Further calculations were carried out to predict the dependence of gas phase evolution on both composition and pressure. Thermodynamic calculations are a valuable tool for the design of these industrially important alloys. Input from experimental data has enabled the refinement of the initial design criteria such that it should now be possible to propose compositions with high VN hardening but without the risk of porosity.

Keywords nitrogen, phase diagrams, porosity, steel, thermodynamics, vanadium

1. Introduction

Steels containing 8-12 wt.% Cr (9Cr steels) are widely used in the petrochemical industry and in both thermal and nuclear power plants where components are subjected to high temperatures and stresses for up to several decades. One of the critical materials properties for such applications is the resistance to creep, i.e., deformation occurring at less than the room-temperature yield stress due to exposure to high temperatures.

Creep can occur by a number of mechanisms, but under typical power plant conditions, it takes place via a two-stage mechanism consisting of the easy glide of dislocations along slip planes until they encounter obstacles on those planes and the thermally assisted "climb" of the dislocations past the obstacles into new, unobstructed slip planes [1993Eva]. It is therefore desirable, for creep resistance, to introduce a maximum possible number of obstacles into the matrix. One of the ways of achieving this is using a fine, homogeneous precipitation of stable carbide or nitride particles. Among the phases found to be useful in this regard are vanadium and niobium nitrides, which form with the approximate stoichiometry MX or M_4X_3, where M signifies a metallic element and X either carbon or nitrogen. To enable plant operation at higher temperatures, with a consequent gain in energy efficiency, work is under way to identify alloy compositions giving optimized creep resistance.

This paper was presented at the International Symposium on User Aspects of Phase Diagrams, Materials Solutions Conference and Exposition, Columbus, Ohio, 18-20 October, 2004.

V.A. Yardley and **Y. de Carlan,** Commissariat à l'Energie Atomique, Centre d'Etudes de Saclay, SRMA, Bât 453, 91 191 Gif Sur Yvette Cedex, France. Contact e-mail: v.a.yardley.95@cantab.net.

2. Modeling for Optimization of Composition

2.1 Matrix Phases

Figure 1 is a pseudobinary equilibrium phase stability diagram for a Fe-0.46 at.% (0.10 wt.%) C system as a function of chromium content, showing only the matrix phases. This diagram, and all the other phase and property diagrams presented below, was calculated using Thermo-Calc [2002And] with the latest steel database TCFE3. Increasing the chromium content stabilizes the body-centered cubic (bcc) ferrite structure at the expense of the face-centered cubic (fcc) austenite. 9Cr steels undergo, before service, a three-stage treatment consisting of austenitisation, i.e., treatment in the domain of austenite stability to redissolve any precipitate phases formed during solidification; rapid cooling (quenching) to form the metastable martensite structure by a displacive mechanism; and a tempering heat treatment

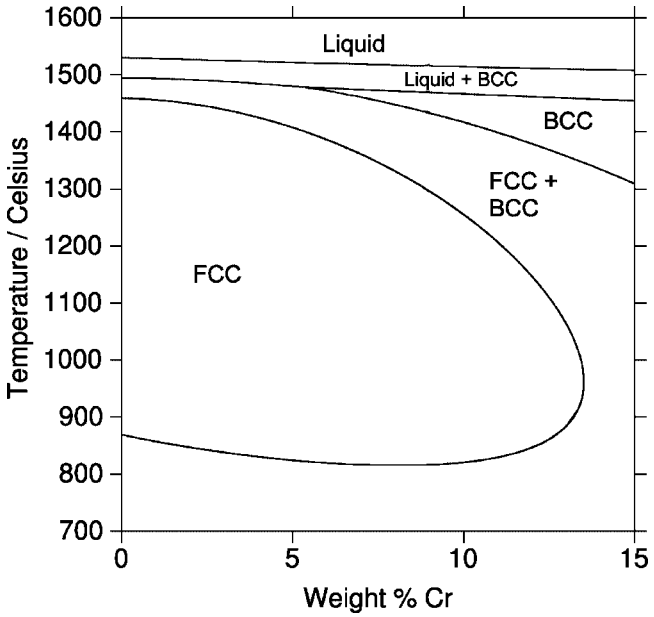

Fig. 1 Pseudobinary phase stability diagram for Fe-0.46at.%(0.10wt.%)C as a function of chromium content

within the low-temperature ferrite stability range to give controlled precipitation of the reinforcing carbonitride phases.

To obtain the desired 100% martensitic microstructure on quenching requires the material to be 100% austenitic at the austenitization temperature. Formation of high-temperature ferrite is to be avoided due to its brittleness. This imposes the requirement that the austenitization temperature and the chromium content must lie within the single-phase fcc "loop" in Fig. 1. A compromise must be reached between high chromium content, favorable for improving oxidation resistance, and high austenitization temperature, necessary to dissolve stable carbide and nitride phases.

In Fig. 2(a), a pseudobinary phase stability diagram for Fe-9.6at.%(9.0wt.%)Cr as a function of carbon content, it can be seen that the effect of carbon is to stabilize fcc austenite. An expanded version of the high-temperature portion of this diagram is given in Fig. 2(b). The small triangle is a three-phase region consisting of liquid, bcc, and fcc, and below this is a "peritectic-like" point (by analogy with a binary diagram) giving a transformation to fcc. The high-temperature bcc phase is termed delta-ferrite, and the low-temperature form, alpha-ferrite.

Pseudobinary phase diagrams can easily be produced for more complex compositions, allowing the effects of other alloying elements on the austenite loop size to be modeled, and compositions to be chosen accordingly.

2.2 Precipitate Phases

Figure 3 shows the temperature of the boundary of the vanadium nitride phase as a function of vanadium content for the composition A2 given in Table 1. Vanadium nitride

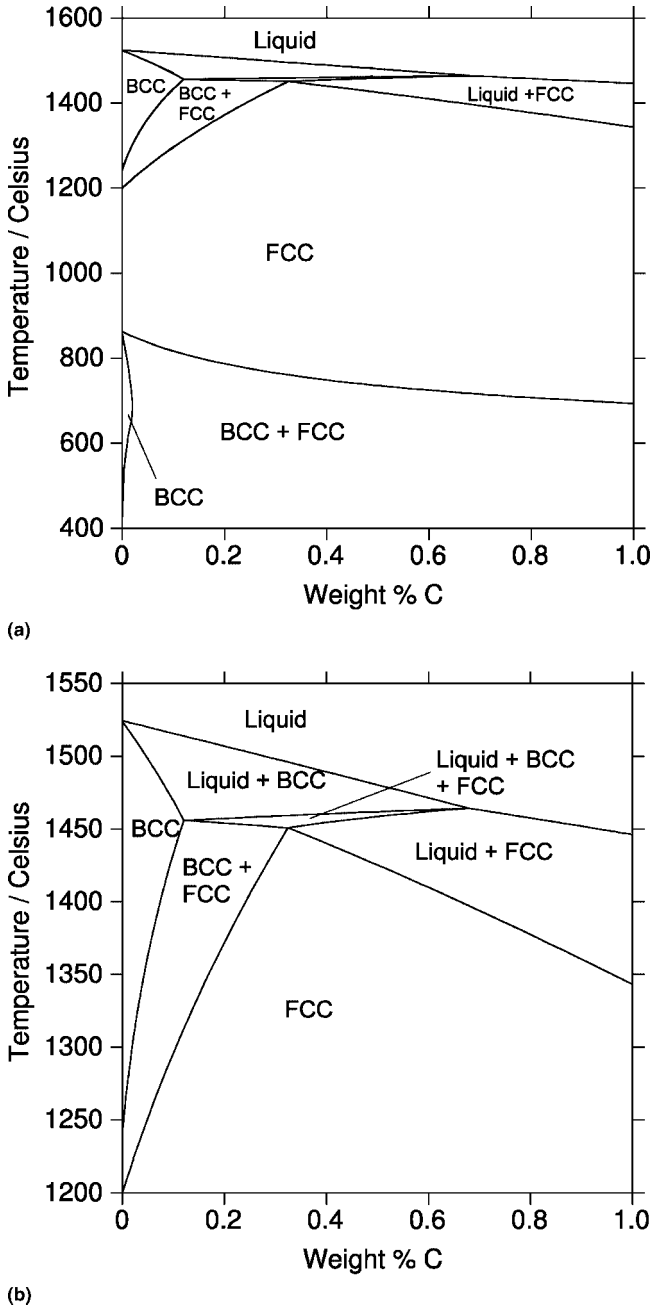

Fig. 2 (a) Pseudobinary phase stability diagram for a Fe-9.6at.%(9.0wt.%)Cr alloy as a function of carbon content (b) Enlargement of (a) for the high-temperature region

is here modeled as a FCC_A1 phase, with a finite solubility for other alloying elements, rather than a stoichiometric compound V_4N_3. In practice, the predicted stoichiometry of the V- and N-rich FCC_A1 phase tends to be close to V_4N_3 in the alloy compositions under consideration [2004Yar]. Within the austenite stability region, Thermo-Calc predicts a monotonic increase of the dissolution temperature with increasing vanadium content. At high V contents, the temperature of dissolution of the nitride phase is close to that of the onset of delta-ferrite formation. This represents an upper

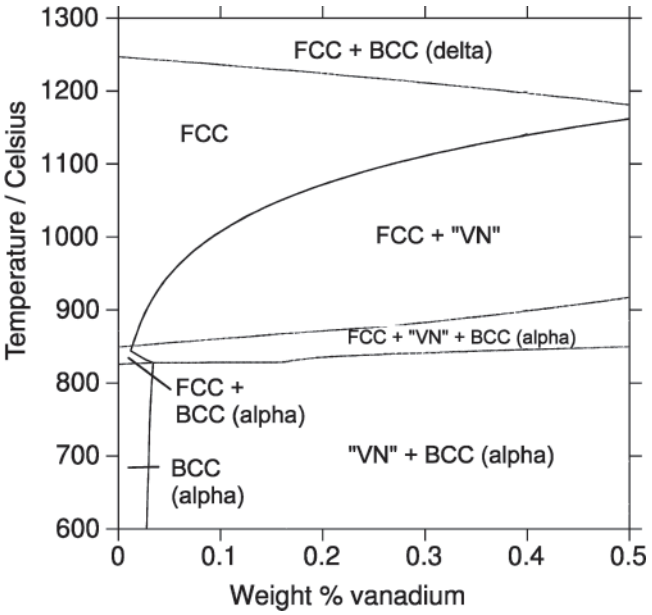

Fig. 3 Variation of dissolution temperature of vanadium nitride phase with temperature for alloy composition A2 (8.53Cr-0.754W-0.343V-0.458C-0.291N at.%)

limit on the allowable concentration of vanadium because delta-ferrite formation during heat-treatment is to be avoided. Similarly, for other MX/M_4X_3 carbonitride formers, the limiting compositions can easily be obtained using thermodynamic modeling software, provided that accurate data for the interactions involved are available in the databases used by the programs.

Carbon favors the formation of the coarse, chromium-rich phase $M_{23}C_6$. This phase does not contribute significantly to secondary phase strengthening and at the same time removes Cr from the matrix, decreasing oxidation resistance. Excessive carbon contents are therefore to be avoided. The equilibrium fraction of $M_{23}C_6$ phase, and the associated matrix Cr content, can also be readily predicted using thermodynamic models.

2.3 Gas Evolution (Porosity)

The allowable nitrogen content may also be limited by the formation of nitrogen gas during solidification. This is predicted by both Thermo-Calc and MTDATA [2002Dav] to be an equilibrium phase at around 1450 °C in high-nitrogen 9Cr steels [those containing 0.2 at.% (0.05 wt.%) N or more]. However, several experimental steels of this type have previously been fabricated without any observation of gas evolution [1991Bra]. Published work exists on the problems of gas evolution in high-nitrogen stainless steels, especially in the area of welding (e.g., [2001Toi, 2004Har]), but there does not seem to be any literature on similar problems in 9Cr steels. However, anecdotal evidence exists that such problems have been encountered.

2.4 Alloy Systems Studied

An example of a 9Cr steel at a mature stage of development is the alloy designated T91 or P91, with a typical composition of Fe-9Cr-0.6Mo-0.2V-0.05Nb-0.2N at.% (8.25Cr-1Mo-0.2V-0.08Nb-0.05N wt.%). There is still scope for improvement on its creep resistance properties, however, and much research has been carried out with this aim.

A number of experimental alloys have been fabricated to study the effects of changing the contents of various alloying elements. Among these are two, designated A1 and A2, in which the vanadium and nitrogen contents were purposely set close to their limiting values as defined in Sec. 2.2 above. This enabled an experimental test of whether this composition could be fabricated without gas evolution. The compositions of all the steels considered are given in Table 1.

3. Experimental Results and Analysis

Macroscopic porosity was observed only in alloys A1 and A2. The pores were up to 10 mm in diameter (Fig. 4). The size and number density of pores was greater in A2 than in A1.

Diagrams of the amounts of each phase present in the systems T91 and A2 as a function of temperature are presented in Fig. 5(a) and (b), respectively. In both cases, the gas phase is predicted to be stable. However, the transformation from liquid to austenite occurs in T91 via the route: liquid + delta-ferrite → delta-ferrite + austenite, but includes an additional stage in A2: liquid + delta-ferrite → delta-ferrite → delta-ferrite + austenite.

The results of the same calculation for the other steels investigated are presented in Table 1 together with the compositions of these alloys. A1 had the same solidification route as A2, with a 100% delta-ferrite stability region, while the other steels in the table showed T91-type solidification characteristics, with the exception of EM10. This, however, is a relatively low-nitrogen steel in which no gas stability region is predicted.

Based on these calculations and observations, porosity seems to be associated with the existence of a temperature range in which gas and delta-ferrite are the only stable phases at equilibrium. This provides us with an 'unacceptability" criterion, allowing us to identify compositions likely to be problematic.

A suggested mechanism for gas formation is as follows: starting in the liquid phase, the first solid to form under equilibrium conditions is delta-ferrite. This has a low solubility for carbon and nitrogen and thus rejects solute into the liquid. Values for nitrogen solubility at 590 °C in pure iron are 8.75 at.% (2.35 wt.%) in the fcc structure and 0.40 at.% (0.10 wt.%) in bcc (taken from [1995Hon]). As the amount of liquid decreases, and more and more solute is rejected into it, its nitrogen content will eventually reach the solubility limit and nitrogen will tend to come out of solution as gas bubbles. Figure 6 shows the solubility limit for each of the phases delta-ferrite, liquid and austenite, when the phase under consideration is in equilibrium only with nitrogen gas, as a function of temperature. The difference between ferrite and the other two phases can clearly be seen.

However, the fact that bubbles do not appear in all systems in which gas is predicted as an equilibrium phase

Table 1 Compositions of steels studied with observations on Thermo-Calc phase diagrams and experiment

	Composition										On calculated phase stability curves		
Designation	C	N	Cr	Mo	W	V	Nb	Ni	Si	Mn	Gas stability domain?	100% delta-ferrite region?	Pores observed?
A1, at.%	0.40	0.330	9.50	…	0.439	0.340	3×10^{-5}	…	…	…	Yes	Yes	Yes
A1, wt.%	0.08	0.083	8.87	…	1.45	0.311	0.005	…	…	…	Yes	Yes	Yes
A2, at.%	0.45	0.291	8.53	…	0.754	0.343	3×10^{-5}	…	…	…	Yes	Yes	Yes
A2, wt.%	0.09	0.072	7.9	…	2.47	0.311	0.005	…	…	…	Yes	Yes	Yes
EM10, at.%	0.44	0.095	9.3	0.628	…	0.03	…	0.17	0.73	0.51	No	Yes	No
EM10, wt.%	0.09	0.024	8.8	1.09	…	0.03	…	0.18	0.37	0.51	No	Yes	No
M1, at.%	0.69	0.079	9.2	0.58	…	…	…	0.54	0.65	0.51	No	No	No
M1, wt.%	0.15	0.02	8.7	1.0	…	…	…	0.57	0.33	0.51	Yes	No	No
M2, at.%	0.50	0.249	9.2	0.58	…	…	…	0.54	0.65	0.51	Yes	No	No
M2, wt.%	0.11	0.063	8.7	1.0	…	…	…	0.57	0.33	0.51	Yes	No	No
M3, at.%	0.45	0.106	9.2	0.31	…	…	…	0.57	0.67	0.51	No	No	No
M3, wt.%	0.09	0.026	8.7	0.53	…	…	…	0.60	0.34	0.51	No	No	No
M5, at.%	0.46	0.073	9.3	0.58	…	…	…	1.06	0.63	0.51	No	No	No
M5, wt.%	0.10	0.018	8.7	1.0	…	…	…	1.12	0.32	0.51	No	No	No
M6, at.%	0.51	0.078	9.0	0.57	…	…	…	0.55	1.37	0.51	No	No	No
M6, wt.%	0.11	0.020	8.5	1.0	…	…	…	0.59	0.70	0.51	No	No	No
T0, at.%	0.46	0.272	9.1	0.57	…	…	0.006	0.08	0.69	0.51	Yes	No	No
T0, wt.%	0.10	0.069	8.6	0.99	…	…	0.01	0.08	0.35	0.51	Yes	No	No
T1, at.%	0.64	0.164	9.1	0.58	…	0.25	0.04	…	0.73	0.51	Yes	No	No
T1, wt.%	0.14	0.041	8.6	1.0	…	0.23	0.07	…	0.37	0.51	Yes	No	No
T3, at.%	0.43	0.280	9.1	0.58	…	…	0.05	0.08	0.69	0.52	Yes	No	No
T3, wt.%	0.09	0.071	8.6	1.00	…	…	0.08	0.08	0.35	0.52	Yes	No	No
T4, at.%	0.43	0.248	9.0	0.57	…	0.22	0.006	0.08	0.69	0.51	Yes	No	No
T4, wt.%	0.09	0.063	8.5	0.99	…	0.20	0.01	0.08	0.35	0.51	Yes	No	No
T5, at.%	0.46	0.279	9.1	…	…	0.25	0.04	…	0.76	0.50	Yes	No	No
T5, wt.%	0.10	0.071	8.6	…	…	0.23	0.07	…	0.39	0.50	Yes	No	No
T91, at.%	0.48	0.201	8.75	0.56	…	0.22	0.045	0.12	0.85	0.37	Yes	No	No
T91, wt.%	0.10	0.051	8.24	0.97	…	0.20	0.075	0.13	0.43	0.37	Yes	No	No

Note: Atomic percentage values were calculated from weight percent values using data in Thermo-Calc database TCFE3.

requires explanation to add rigor to the porosity criterion. This point will be discussed in more detail in Sec. 5.

4. Compositional Effects on Phase Stabilities

Assuming that the porosity criterion proposed above is valid, the effect of alloying element concentrations on the tendency to porosity was investigated. Pseudobinary phase diagrams illustrating the effect of the concentrations of various elements on the domains of phase stability in A2 are shown in Fig. 7(a)-(i). In each case, the basis composition is the original composition of alloy A2, and only the content of the element of interest is varied. The zone of particular interest is the bcc + gas domain believed to be associated with porosity. There are several groupings of effects, summarized below, which are broadly consistent with the known ferrite- or austenite-stabilizing properties of these elements.

- W (7a) and Mo (7b) are strong ferrite formers, which favor both delta-ferrite and gas.

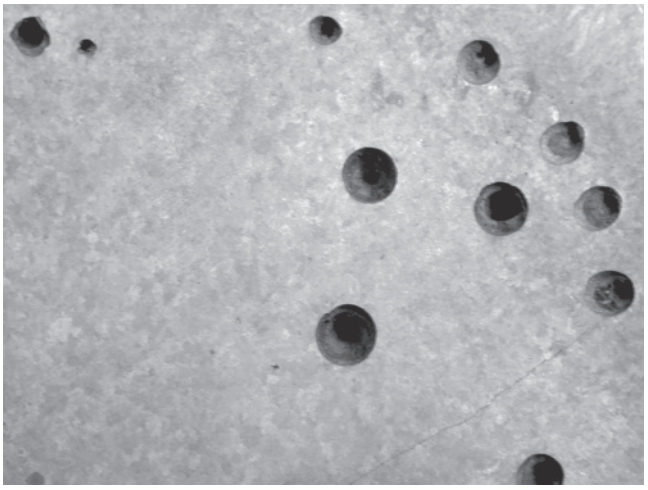

Fig. 4 Micrograph of alloy A1 (9.50Cr-0.439W-0.340V-0.408C-0.330N at.%), showing porosity. The diameter of the largest pores is approximately 10 mm.

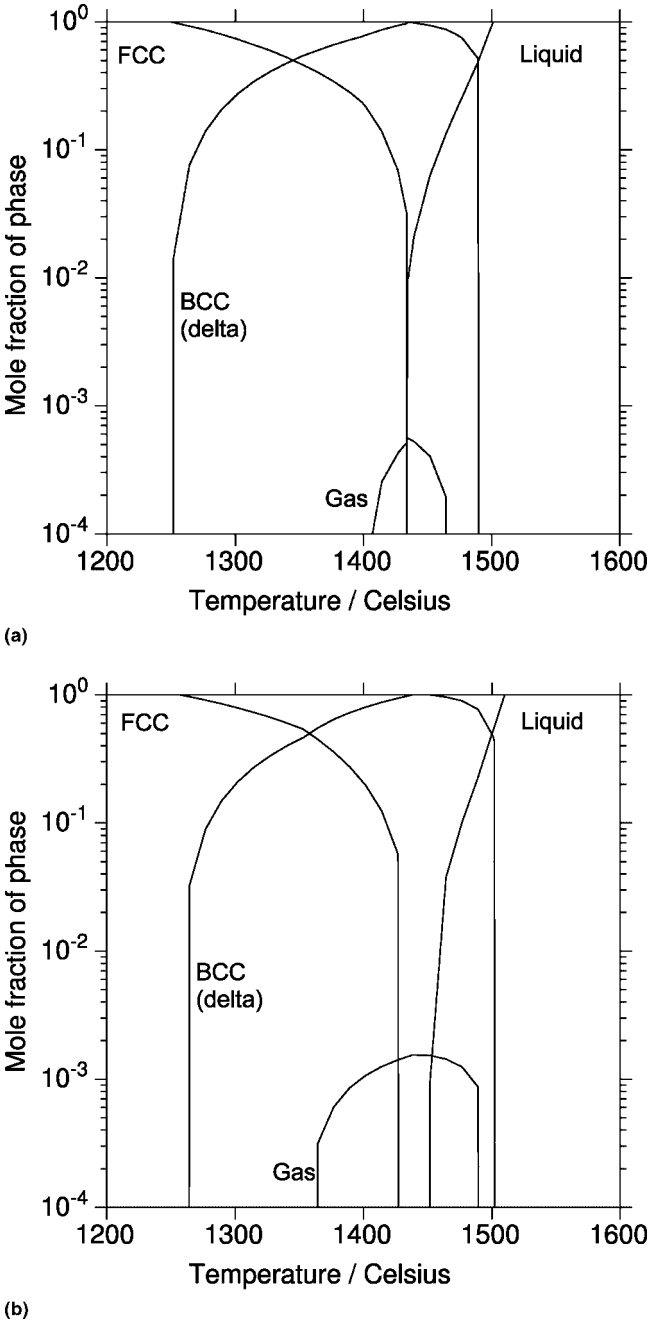

Fig. 5 (a) Mole fraction of phases versus temperature in alloy T91 (8.75Cr-0.56Mo-0.22V-0.045Nb-0.483C-0.201N-0.12Ni-0.85Si-0.37Mn at.%) (b). Mole fraction of phases versus temperature in alloy A2 (8.53Cr-0.754W-0.343V-0.458C-0.291N at.%)

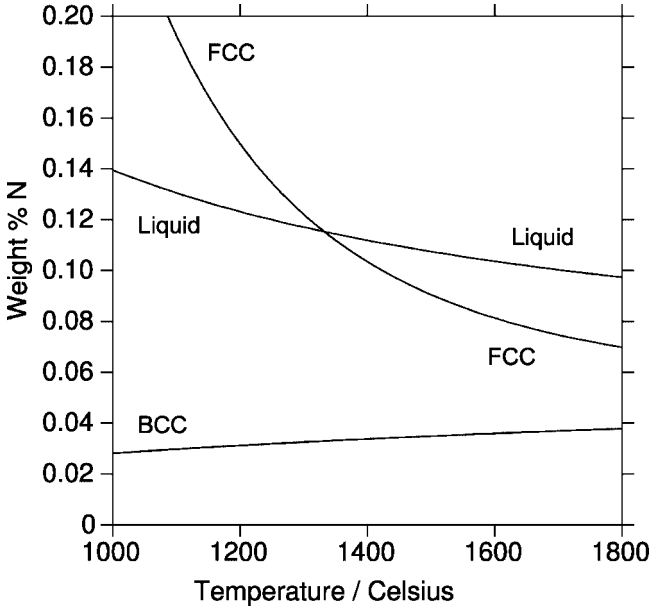

Fig. 6 Nitrogen solubility limits for each of the phases delta-ferrite, liquid, and austenite when the phase under consideration is in equilibrium only with nitrogen gas

- Cr (7c) stabilizes delta-ferrite but also increases the solubility of nitrogen in ferrite, leading to a wider delta-ferrite domain but a narrower gas domain at high Cr content.
- Si (7d) and V (7e) are known as ferrite stabilizers but have a negligible effect on the phase domains in the concentrations of interest here.
- Mn (7f) and Ni (7g) are austenite stabilizers, which decrease both the delta-ferrite and gas stability regions. An addition of just under 0.4 wt.% Ni to the A2 composition is sufficient to suppress the bcc + gas two-phase domain.
- C (7h) is also an austenite stabilizer, with a stronger effect per unit mass than Mn or Ni. The bcc + gas domain disappears above a critical concentration of 0.1 wt.% C in A2.
- N (7i), as expected, favors gas formation. The critical nitrogen content for gas stability is lowest when the matrix phase is 100% bcc.

Avoidance of porosity therefore requires, in general terms, a decrease in the concentration of ferrite-stabilizers and/or an increase in that of austenite-stabilizers. However, there are disadvantages to such a modification: the ferrite-stabilizers Cr, Mo, and W play important roles in the material properties, and increasing the carbon content would favor the formation of coarse $M_{23}C_6$ precipitates, reducing the matrix Cr content, as discussed above. Increasing the Mn and Ni contents appears beneficial for the avoidance of porosity, but these elements are believed to decrease creep resistance [2004Car]. Whether this effect would be outweighed by the gain in creep strength provided by a maximized vanadium nitride concentration remains to be determined.

5. Constraints on Gas Evolution

The porosity criterion proposed above, while it may be a useful "rule of thumb," does not provide any explanation of why a 100% delta-ferrite region seems to be required for the formation of gas in practice. A more rigorous understanding of why this is so would enable a more thorough validation

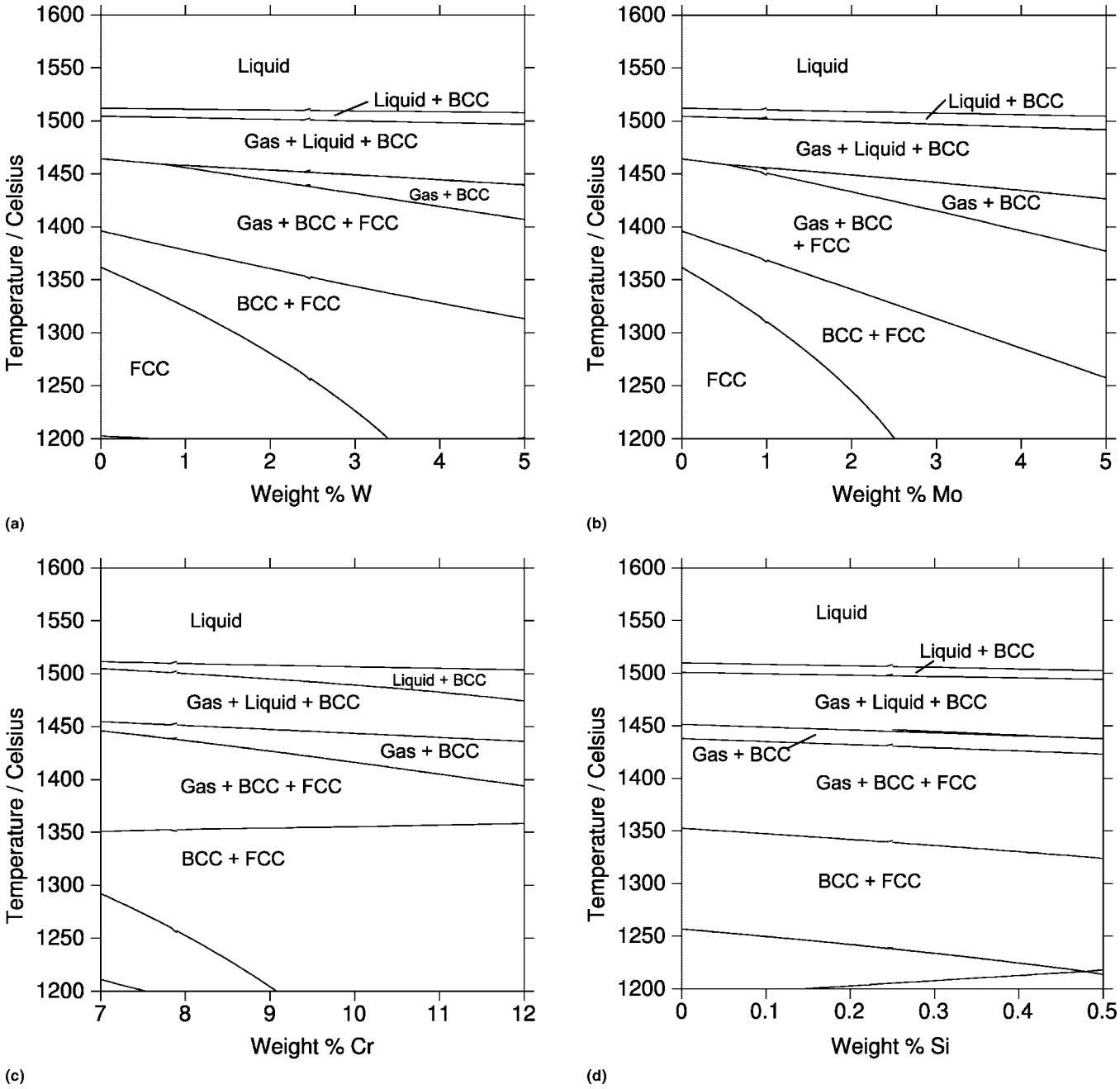

Fig. 7 Pseudobinary phase stability diagrams for alloy A2 (8.53Cr-0.754W-0.343V-0.458C-0.291N at.%) as a function of the concentration of: (a) tungsten (b) molybdenum (c) chromium (d) silicon (e) vanadium (f) manganese (g) nickel (h) carbon (i) nitrogen (continued)

of the criterion than is possible with the small number of experimental data available to us at present.

Three possible approaches to this issue have been considered: the effect of pressure and capillarity on the formation of gas bubbles, simulation of solidification using a Scheil-Gulliver approach, and consideration of the kinetics of delta-ferrite formation.

5.1 Pressure and Capillarity

One of the reasons why gas is not observed in practice in many of the systems in which it is predicted may be that the effective pressure experienced by a gas bubble nucleating in a liquid metal will be greater than atmospheric pressure if there is a column of liquid metal above it. The pressure difference caused by this is ΔP_{column}:

$$\Delta P_{column} = \rho g h \quad \text{(Eq 1)}$$

where ρ is the density of the metal, g the acceleration due to gravity, and h the height of the column of liquid.

In addition, a bubble will experience an excess pressure due to the curvature of its interface with the matrix and the

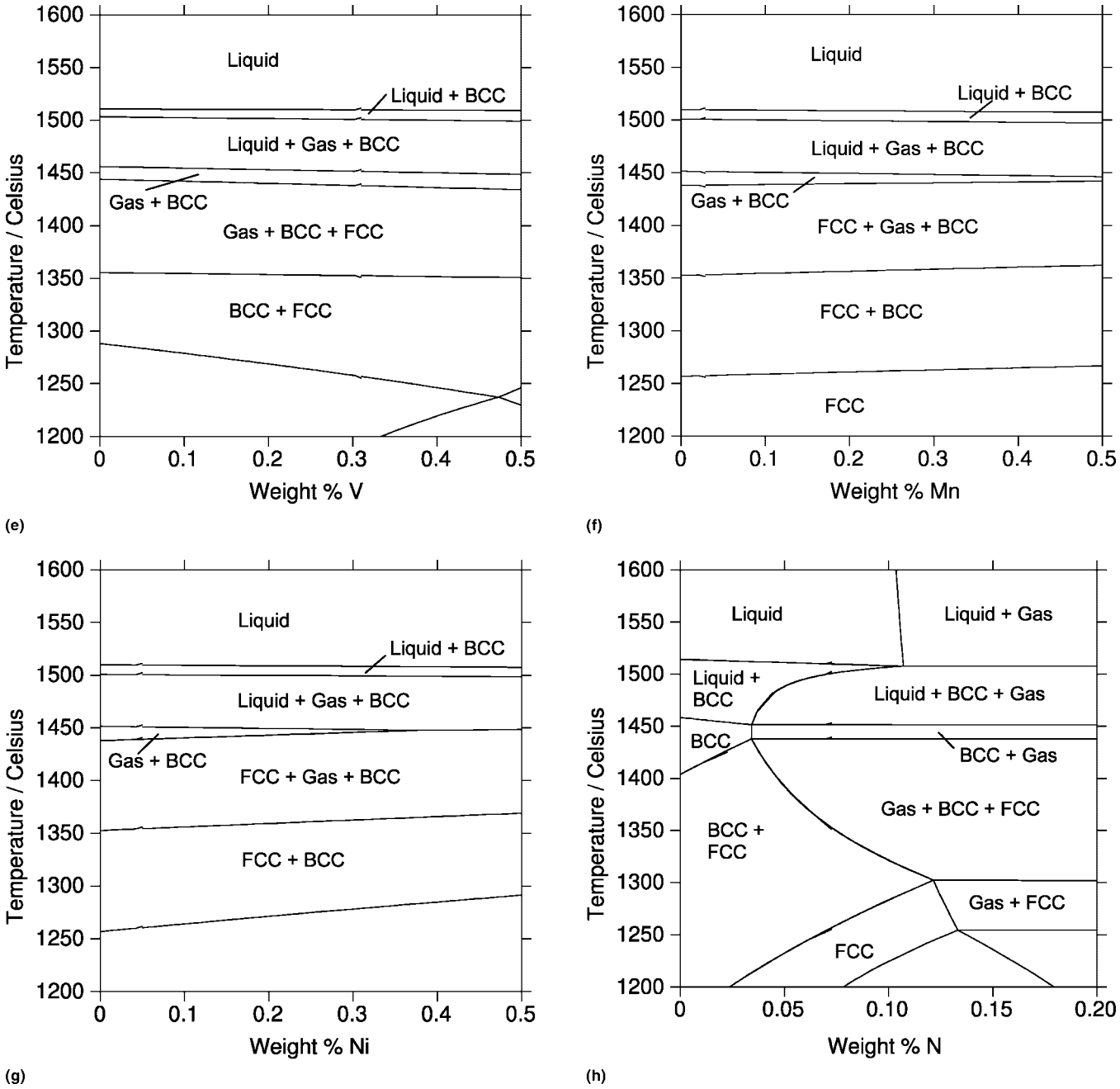

Fig. 7 (cont.) Pseudobinary phase stability diagrams for alloy A2 (8.53Cr-0.754W-0.343V-0.458C-0.291N at.%) as a function of the concentration of: (a) tungsten (b) molybdenum (c) chromium (d) silicon (continued) (e) vanadium (f) manganese (g) nickel (h) carbon (i) nitrogen

energy of this interface. This pressure difference ΔP_{capill} is given approximately:

$$\Delta P_{capill} = \frac{2\gamma}{r} \quad \text{(Eq 2)}$$

where r is the radius of a spherical bubble and γ the energy of its interface with the liquid [1992Por]. These two pressure terms will both tend against the formation of a stable gas bubble.

Taking the density of the liquid steel as 7.8×10^3 kg m^{-3}, it was calculated that the liquid column height required to give a ΔP_{column} value of 1×10^5 Pa was around 1.3 m. Considering that solidification occurs quickly, such a height of liquid metal above a prospective bubble is unlikely. No numerical estimates of the gas-liquid interfacial energy in steel have so far been found, so an estimate of ΔP_{capill} could not be made.

Thermo-Calc equilibrium calculations predicted that increasing the pressure of the system reduces the tendency for gas formation, as would be expected. Approximately four times atmospheric pressure was required to avoid the ap-

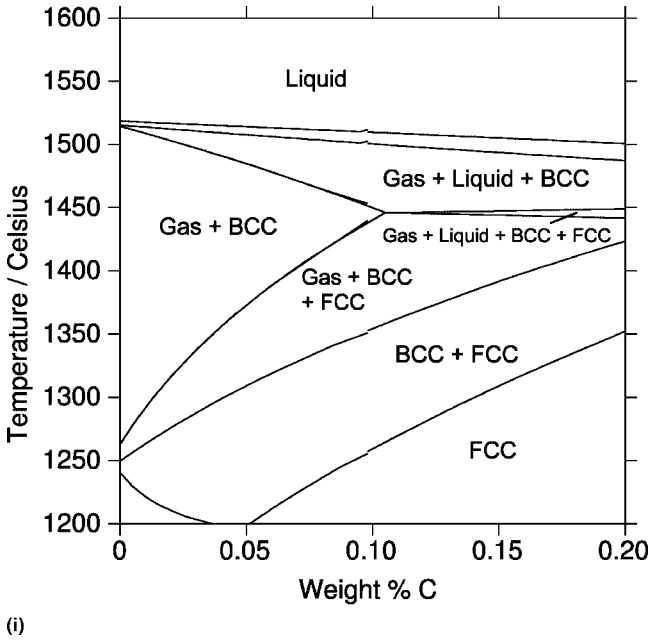

(i)

Fig. 7 (cont.) Pseudobinary phase stability diagrams for alloy A2 (8.53Cr-0.754W-0.343V-0.458C-0.291N at.%) as a function of the concentration of: (a) tungsten (b) molybdenum (c) chromium (d) silicon (e) vanadium (f) manganese (g) nickel (h) carbon (i) nitrogen

pearance of gas as a stable phase at equilibrium in alloy A2 [2004Yar]. Calculations of the minimum pressure needed to avoid gas stability were performed in Thermo-Calc by removing the condition on pressure (P = none) and setting a condition that the number of moles of gas phase be fixed at zero. This determines the pressure at the boundary of the gas phase stability domain.

Figure 8 shows the variation of this limiting pressure value as a function of temperature for alloys T91 and A2. In Fig. 8(a), it can be seen that around twice the pressure is required to avoid the gas phase in A2 than in T91. Comparing Fig. 8(a) and Fig. 5(a) and (b) shows that the peaks of these pressure curves occur in the temperature range of transition from liquid to austenite, which is accompanied by a maximum in the delta-ferrite fraction.

In Fig. 8(b), the effect of changing the carbon content of A2 on this pressure condition is presented. Increasing carbon decreases the pressure required to maintain nitrogen in solution.

Figure 8(c) shows the effect of the nitrogen content (note the difference in vertical scale from the other figures). One of the principal compositional differences between T91 and A2 is the nitrogen content of 0.20 at.% (0.05 wt.%) in T91 as compared with 0.29 at.% (0.07 wt.%) in A2. This, alone, may be sufficient to account for the differences in peak heights in Fig. 9(a).

Finally, Fig. 8(d) illustrates that the tungsten content has very little effect on this condition, apart from a broadening of the peak, which is consistent with the increased delta-ferrite stability range with increasing ferrite-stabilizer content.

The same calculation was performed for the high-nitrogen 9Cr steels in Table 1. The highest minimum pressure calculated for a porosity-free steel was just over 3.5 times atmospheric pressure. This value could be used as an additional indicator of the likely tendency of an alloy composition to present porosity problems on solidification.

It is clear from the above calculations that if the alloy fabrication process were to be carried out at a sufficiently high pressure, gas formation could be avoided. However, this type of processing would increase production costs so may not be commercially viable.

5.2 Scheil-Gulliver Solidification Simulation

The second approach used was a simulation of the solidification process using a Scheil-Gulliver model. This is available as a module in Thermo-Calc and is described in detail in [2004Shi]; its basic principles are that there is no diffusion in solid phases, but perfect mixing in the liquid, and that local equilibrium holds at the interface between liquid and solid [1992Por]. These assumptions are most likely to be valid for rapid cooling.

The calculation is performed by first determining the liquidus temperature, then decreasing the temperature by a small amount and recalculating the equilibrium. This results in the appearance of a certain amount of solid, and a partitioning of elements between the solid and liquid phase. The resulting modified liquid composition is taken as the starting point for the next iteration of the calculation, while the components partitioned into the solid are considered to be frozen-in and to take no further part in the equilibrium. Iterations are performed until the liquid phase is consumed.

Plots of quantities obtained from this model for A2 and T91 are shown in Fig. 9. Figure 9(a) shows the incremental mass of gas evolved at each temperature step for calculations performed at different pressures on A2. Increasing the pressure decreases the temperature range over which gas is evolved both at the upper and lower limits and also decreases the quantity of gas produced. The masses of delta-ferrite and austenite produced are given in Fig. 9(b). These did not vary significantly with the pressure, so only the curves for atmospheric pressure are shown. According to this model, in which solid-state phase transformations are not permitted, the vast majority of the microstructure will be ferritic.

Curves for T91 are presented in Fig. 9(c) and (d). The mass of gas evolved at 1×10^5 Pa is about a third that of A2, and there is no gas at all at 4×10^5 Pa. Both the liquidus and the low-temperature limit of delta-ferrite evolution occur at temperatures lower than that for A2, but otherwise the solid phase formation behavior of the two alloys seems very similar, despite the differences in their equilibrium phase stability diagrams.

The original Scheil model implemented in Thermo-Calc does not appear to take explicit account of the gas phase; instead, all non-liquid phases are treated as if they were solid. A newer version of the Scheil module, in which diffusion of the interstitial species C and N could be considered if desired, appeared to offer a solution to this, since it would, it was presumed, allow back-diffusion of nitrogen from the gas into the liquid and solid phases. However, attempts at using this model with N as a fast-diffusing species failed because the calculation "crashed" when the gas

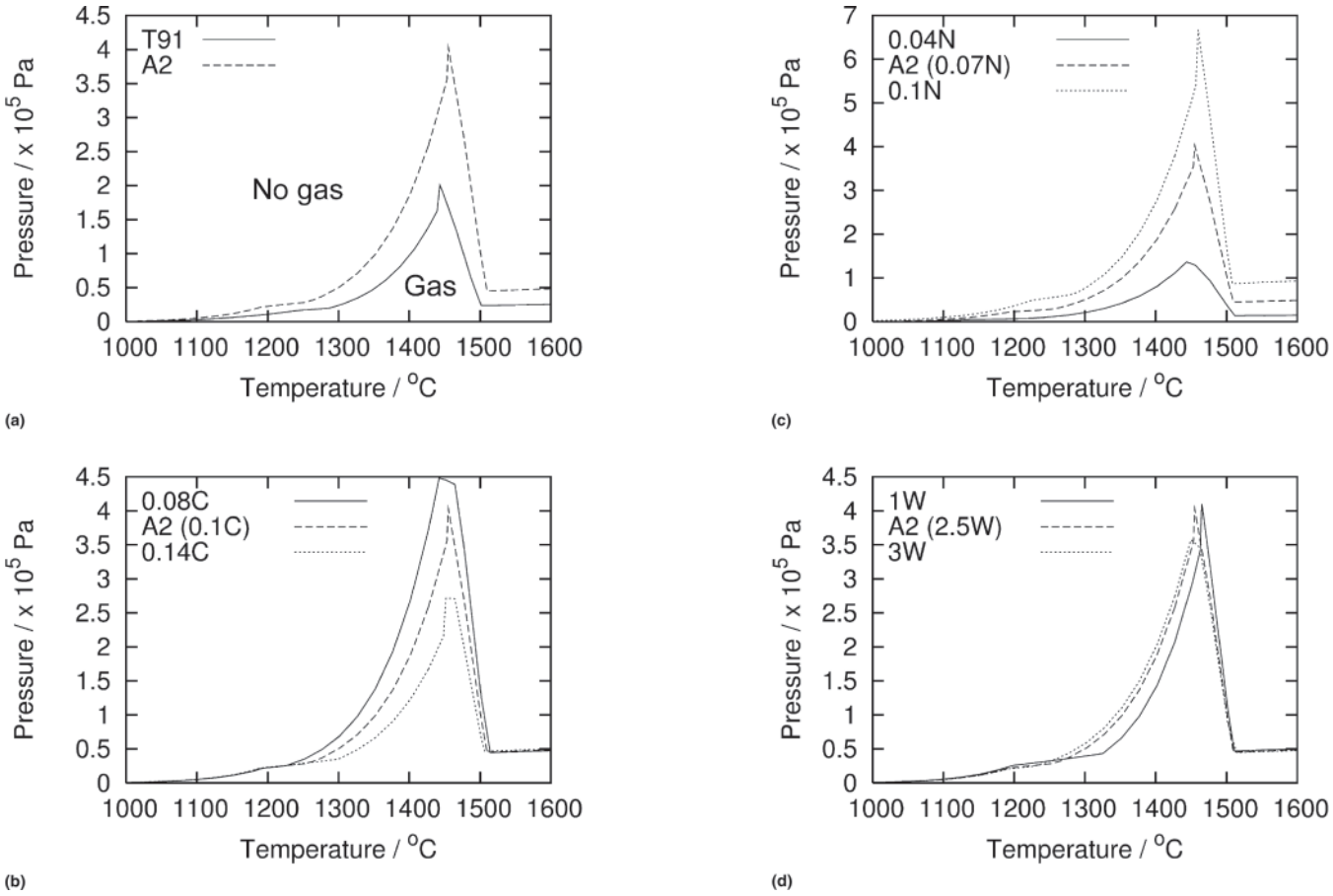

Fig. 8 Variation of the limiting pressure for the avoidance of gas formation as a function of temperature for: (a) the compositions T91 and A2, (b) A2 with modified carbon content, (c) A2 with modified nitrogen content, (d) A2 with modified tungsten content. All concentrations in wt.%

phase was encountered. This appears to be a systematic effect because it occurs even with deliberately chosen, very simple high-nitrogen systems, so this type of modeling had to be abandoned. The model without interstitial diffusion is considered to be of limited validity for modeling the solidification of interstitial-containing systems [2004Shi].

5.3 Kinetics of Delta-Ferrite Formation

A final possible explanation for the lack of gas in certain cases concerns the kinetics of formation of delta-ferrite. If this phase is prevented from appearing, the solubility limit for nitrogen in the two other phases, liquid and austenite, is never exceeded for equilibrium solidification of A2 (Fig. 6). Figure 10, calculated for the A2 composition with the bcc phase suspended, confirms that no gas is expected in this case. Equally, if delta-ferrite were present, but in sufficiently small quantities, gas formation would be avoided.

A study on the welding of T91-type alloys showed that some delta-ferrite was observed in weld metals where a 100% delta-ferrite region was predicted at equilibrium; little or none was observed otherwise [2004Rab]. The cooling rate, in this case, is very high, so it can be assumed that the high-temperature microstructure in the melted zone is frozen-in and that the microstructure observed at room temperature in welds is an accurate reflection of the phases present at high temperature. Delta-ferrite thus seems only to appear, with possible consequences for gas evolution, in systems that have an equilibrium temperature range in which it is the only stable matrix phase. It must be borne in mind that the cooling rate for castings may be lower than those for the welds, so the results may not be directly transferable to the issue of porosity on solidification. However, the implication seems to be that considerably less delta-ferrite is formed than is predicted by the Scheil-Gulliver model. This may be because the delta-ferrite does not have sufficient time to nucleate before the temperature decreases to such a point as it is no longer stable.

While these three approaches have provided some insight into the dependence of gas evolution on composition, it has not been possible, using the available models, to make a simulation that correctly predicts whether porosity will appear on solidification.

6. Conclusions

A number of experimental steel compositions based on the existing material T91 were fabricated with the aim of

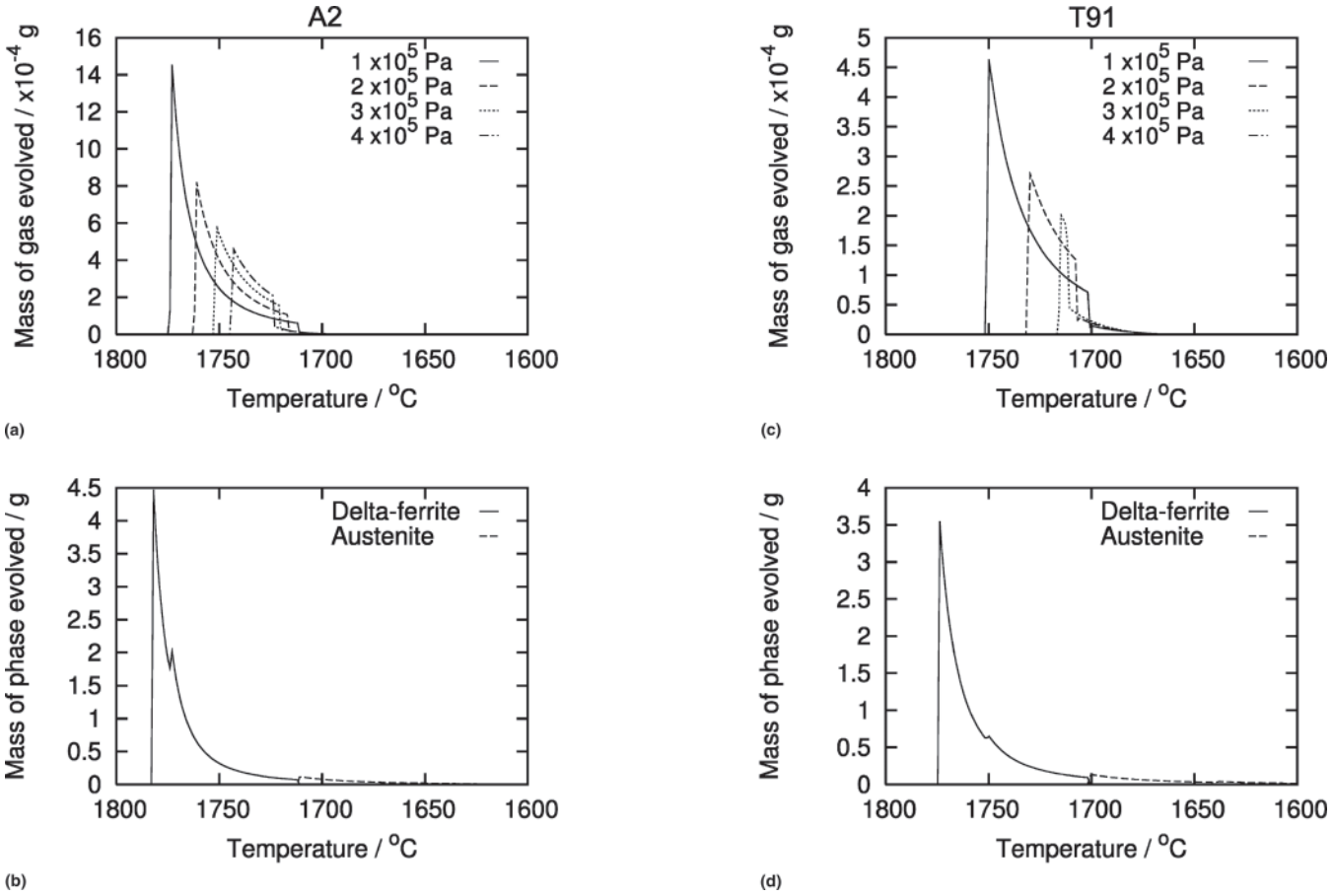

Fig. 9 Results of Scheil-Gulliver solidification model for steels A2 and T91: (a) mass of gas evolved on solidification of A2 at various pressures, (b) corresponding mass of delta-ferrite and austenite phases produced at 1×10^5 Pa, (c) mass of gas evolved on solidification of T91 at various pressures, (d) corresponding mass of delta-ferrite and austenite phases produced at 1×10^5 Pa

investigating the effect of compositional modification, and in particular, determining the maximum amount of nitrogen that could be added without causing fabricability problems. Two of the experimental alloys were found to contain macroscopic porosity, but the others were porosity-free. The compositional origins of porosity were investigated using equilibrium phase stability calculations; this led to the establishment of a criterion that a temperature range in which gas and delta-ferrite are the only stable phases tends to lead to porosity and should be avoided. The influence of composition on the existence and extent of this region was studied, demonstrating that it is favored by ferrite-stabilizing elements and suppressed by austenite-stabilizers.

In many of the higher-nitrogen 9Cr alloys, gas was predicted as an equilibrium phase, but porosity was not observed in practice. Reasons for this were considered, with the aim of adding rigor to the porosity criterion. One of the more useful results is that the pressure required to maintain nitrogen in solution, avoiding gas formation, is considerably lower in the porosity-free alloys. A limiting value of this pressure could be used as a further criterion to try to predict the occurrence of porosity in proposed alloy systems. Solidification simulations using the Scheil-Gulliver model were less conclusive, partly due to the difficulty of taking

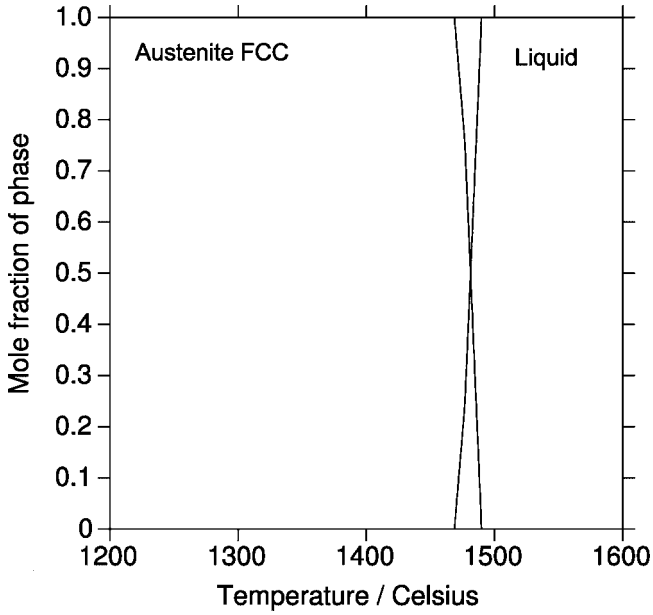

Fig. 10 Mole fraction of phases in A2 (8.53Cr-0.754W-0.343V-0.458C-0.291N at.%) calculated with bcc phase suspended

into account the gas phase, but were in agreement that increasing the pressure tends to suppress gas formation and that much less gas was predicted for porosity-free than for porous alloy systems. Observations of weld microstructures suggested that delta-ferrite formed more readily in compositions in which a temperature range existed over which it was the only stable phase. This led to the suggestion that the kinetics of delta-ferrite formation may also play a part in the appearance or otherwise of the gas phase.

The calculation of equilibrium phase diagrams has been found to be very useful in designing and understanding new 9Cr steel compositions and even, to some extent, providing insight into the non-equilibrium phenomenon of gas evolution on solidification. It was not possible, using the Scheil-Gulliver model, to obtain a simulation capable of predicting correctly whether porosity would occur on solidification of a given alloy. However, the porosity criteria established on the basis of equilibrium calculations and experimental observations should aid in the identification of high-nitrogen compositions likely to pose a risk of porosity.

7. Summary

Fe-8-12Cr ferritomartensitic steels used for high-temperature applications can be strengthened with vanadium nitride (VN) precipitates. However, this requires a high nitrogen content, which could cause porosity during fabrication. Using phase stability calculations and experimental results, a porosity criterion has been determined. This should facilitate future alloy design.

Acknowledgment

The authors would like to thank Dr. Jean-Christophe Brachet for helpful discussions on many aspects of this work.

References

2002And: J-O. Andersson, T. Helander, L. Hoglund, P. Shi, and B. Sundman, THERMO-CALC & DICTRA, Computational Tools For Materials Science, *Calphad,* 2002, 26 (2), p 273-312

1991Bra: J-C. Brachet, Martensitic 9Cr-1Mo Alloys: Effects of Nitrogen, Niobium and Vanadium Additions on the Microstructure, Phase Transformations and Mechanical Properties, Ph.D. Thesis, Université de Paris-Sud, Paris, France, 1991, in French

2004Car: Y. de Carlan, M. Murugananth, T. Sourmail, and H.K.D.H. Bhadeshia, Design of New Fe-9CrWV Reduced-Activation Martensitic Steels for Creep Properties at 650 °C, *J. Nucl. Mater.,* 2004, Vol 329-333, p 238-244

2002Dav: R.H. Davies, A.T. Dinsdale, J.A. Gisby, J.A.J. Robinson, and S.M. Martin, MTDATA—Thermodynamic and Phase Equilibrium Software from the National Physical Laboratory, *Calphad* 2002, 26 (2), p 229-271

1993Eva: R.W. Evans and B. Wilshire, Introduction to Creep, Oakdale Publishing Company for The Institute of Materials, 1993

2004Har: M. Harzenmoser, Review: Welding of High Nitrogen Steels, *Materials and Manufacturing Processes,* 2004, 19 (1), p 75-86

1995Hon: R.W.K. Honeycombe and H.K.D.H. Bhadeshia, Steels: Microstructure and Properties (2nd ed.), Edward Arnold, 1995, p 6

1992Por: D.A. Porter and K.E. Easterling, Phase Transformations in Metals and Alloys, 2nd ed., Chapman and Hall, 1992

2004Rab: V. Rabeau, Y. de Carlan, and V.A. Yardley, Commissariat à l'Energie Atomique, Centre d'Etudes de Saclay, SRMA, Bât 453, 91 191 Gif Sur Yvette Cedex, France, unpublished work, 2004

2004Shi: P. Shi, Ed., Thermo-Calc Software Users' Guide, Version Q, 2004, Foundation of Computational Thermodynamics, Stockholm, Sweden, p 336-342

2001Toi: M. Du Toit, The Behaviour of Nitrogen during the Autogenous ARC Welding of Stainless Steel, Ph.D. Thesis, University of Pretoria, South Africa, 2001, http://upetd.up.ac.za/thesis/available/etd-09132002-100245/

2004Yar: V.A. Yardley, Commissariat à l'Energie Atomique, Centre d'Etudes de Saclay, SRMA, Bât 453, 91 191 Gif Sur Yvette Cedex, France, unpublished work, 2004